Dimerization of HIV-1 protease occurs through two steps relating to the mechanism of protease dimerization inhibition by darunavir

Hironori Hayashi[a,b], Nobutoki Takamune[c], Takashi Nirasawa[d], Manabu Aoki[a,e], Yoshihiko Morishita[d], Debananda Das[b], Yasuhiro Koh[a], Arun K. Ghosh[f], Shogo Misumi[c], and Hiroaki Mitsuya[a,b,1]

[a]Departments of Hematology, Rheumatology, and Infectious Disease, Kumamoto University Graduate School of Medicine, 1-1-1 Honjo, Chuo-ku, Kumamoto 860-8556, Japan; [b]Experimental Retrovirology Section, HIV and AIDS Malignancy Branch, National Cancer Institute, National Institutes of Health, Bethesda, MD 20892; [c]Department of Biochemistry, Kumamoto University Graduate School of Pharmaceutical Sciences, 5-1 Ooehonmachi, Chuo-ku, Kumamoto 862-0973, Japan; [d]Bruker Daltonics K.K., 3-9 Moriya, Kanagawa-ku, Yokohama 221-0022, Japan; [e]Department of Medical Technology, Kumamoto Health Science University, 325 Izumi-cho, Kita-ku, Kumamoto 861-5598, Japan; and [f]Departments of Chemistry and Medicinal Chemistry, Purdue University, West Lafayette, IN 47907

Edited* by Yoshihiro Kawaoka, University of Wisconsin–Madison, Madison, WI, and approved June 27, 2014 (received for review January 2, 2014)

Dimerization of HIV-1 protease (PR) subunits is an essential process for PR's acquisition of proteolytic activity, which plays a critical role in the maturation of HIV-1. Recombinant wild-type PR (PR^{WT}) proved to dimerize, as examined with electrospray ionization mass spectrometry; however, two active site interface PR mutants (PR^{T26A} and PR^{R87K}) remained monomeric. On the other hand, two termini interface PR mutants ($PR^{1\text{-}C95A}$ and $PR^{97/99}$) took both monomeric and dimeric forms. Differential scanning fluorimetry indicated that $PR^{1\text{-}C95A}$ and $PR^{97/99}$ dimers were substantially less stable than PR^{WT} dimers. These data indicate that intermolecular interactions of two monomers occur first at the active site interface, generating unstable or transient dimers, and interactions at the termini interface subsequently occur, generating stable dimers. Darunavir (DRV), an HIV-1 protease inhibitor, inhibits not only proteolytic activity but also PR dimerization. DRV bound to protease monomers in a one-to-one molar ratio, inhibiting the first step of PR dimerization, whereas conventional protease inhibitors (such as saquinavir) that inhibit enzymatic activity but not dimerization failed to bind to monomers. DRV also bound to mutant PRs containing the transframe region-added PR (TFR-PR^{D25N} and TFR-$PR^{D25N\text{-}7AA}$), whereas saquinavir did not bind to TFR-PR^{D25N} or TFR-$PR^{D25N\text{-}7AA}$. Notably, DRV failed to bind to mutant PR containing four amino acid substitutions (V32I, L33F, I54M, and I84V) that confer resistance to DRV on HIV-1. To our knowledge, the present report represents the first demonstration of the two-step PR dimerization dynamics and the mechanism of dimerization inhibition by DRV, which should help design further, more potent novel PIs.

AIDS | thermal stability | two-step dimerization dynamics | protease precursor

Dimerization of HIV-1 protease (PR) subunits is an essential process for the acquisition of proteolytic activity of PR, which plays a critical role in viral maturation in the replication cycle of HIV-1 (1, 2). Thus, PR dimerization inhibition is likely to abolish proteolytic activity and should serve as a promising target for HIV-1 intervention. Structurally there are two interfaces, which operate in the efficient PR dimerization. One is the termini interface, and the other is the active site interface (3, 4). The termini interface comprises four antiparallel β-sheets involving the first four amino- and carboxy-termini residues of both subunits. Todd et al. (5) have reported that the binding force generated by the termini interface contributes close to 75% of the entire dimerization energy. Indeed, Ishima and others have demonstrated that three amino acid substitutions (T26A, D29N, and R87K), located at the active site interface, together with C-terminal truncation of four amino acids (96–99), effectively disrupted PR dimerization as examined with NMR spectroscopy (Fig. 1) (6–8). Various groups have tried to target the termini interface in an attempt to intervene HIV-1 replication (9–12); however, none of such efforts to disrupt the termini interface interactions have led to clinical applications. On the other hand, the most recently US Food and Drug Administration (FDA)-approved PR inhibitor (PI), darunavir (DRV), is (to our knowledge) the first to be shown to block the dimerization of HIV-1 PR, as examined with the intermolecular FRET-based HIV-expression assay (Fig. S1) (13). Furthermore, a combination of four amino acid substitutions in the proximity of the active site interface (V32I/L33F/I54M/I84V), which emerged in PR when HIV-1–infected individuals were heavily treated with multiple PR inhibitors (PIs) and failed such treatment and when HIV-1 was selected in vitro in the presence of increasing concentrations of DRV (14), has been shown to decrease the dimerization inhibition activity of DRV (Fig. 1 and Fig. S1*B*) (15). However, the dynamics of dimerization of PR subunits, as well as the molecular mechanism of DRV inhibition of PR dimerization, remain to be elucidated.

Here we generated a variety of recombinant PR species with various amino acid substitution(s) and/or deletions introduced

Significance

Dimerization of HIV-1 protease (PR) plays a critical role in the replication of HIV-1. Darunavir (DRV) inhibits not only proteolytic activity but also PR dimerization. The present study shows that PR dimerization process undergoes two steps and that DRV inhibits the first step of PR dimerization by binding to PR monomers in a one-to-one molar ratio. The present study also demonstrates that DRV binds to a transframe precursor PR protein, indicating that DRV's monomer binding is involved in the Gag-Pol autoprocessing inhibition. To our knowledge, the present report represents the first demonstration of the two-step PR dimerization dynamics and the mechanism of dimerization inhibition by DRV, which should help design further, more potent novel PR inhibitors.

Author contributions: H.H. and H.M. designed research; H.H., N.T., T.N., M.A., and Y.M. performed research; N.T., M.A., Y.M., and A.K.G. contributed new reagents/analytic tools; H.H., N.T., T.N., D.D., Y.K., S.M., and H.M. analyzed data; and H.H. and H.M. wrote the paper.

Conflict of interest statement: A.K.G. and H.M. are coinventors on a US government patent for darunavir. H.M. is an employee of the US government and is named so under the terms of the Federal Technology Transfer Act. All rights, title, and interest to the patent have been assigned to the US government, which may give a part of the royalties the government receives to its inventors.

*This Direct Submission article had a prearranged editor.

[1]To whom correspondence should be addressed. Email: hmitsuya@helix.nih.gov.

This article contains supporting information online at www.pnas.org/lookup/suppl/doi:10.1073/pnas.1400027111/-/DCSupplemental.

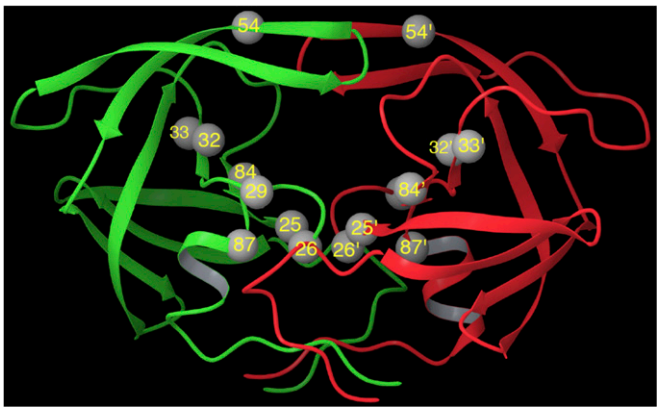

Fig. 1. Locations of major amino acid substitutions examined in the present study. V32I, L33F, I54M, and I84V are associated with HIV-1's DRV resistance. T26, D29, and R87 are known to be critical for PR dimerization. D25N is inserted to inactivate the enzymatic activity of HIV-1 PR.

and examined whether such mutated PR species interacted and dimerized using electrospray ionization mass spectrometry (ESI-MS) (16, 17). We also asked how PIs, including DRV, interacted with such various PR species and blocked the dimerization of PR subunits. The present data demonstrate that intermolecular interactions of two monomers occur first at the active site interface, generating weakly dimerized subunits (transient dimers), and that interactions at the termini interface subsequently occur, generating stable dimers. The ESI-MS data also show that DRV binds to PR monomers in a one-to-one molar ratio and inhibits the first step of PR dimerization, whereas conventional PIs (such as saquinavir) fail to bind to monomers. To our knowledge, the present report should represent the first demonstration of the two-step PR dimerization dynamics and the mechanism of dimerization inhibition by DRV.

Results

The ESI-MS spectra of PR^{WT} and PR^{D25N} revealed four peaks of differently charged ions in the range of mass/charge ratio (m/z) of 1,500–2,500 (Fig. 2 *A* and *B*). Because +5 charged monomer ion and +10 charged dimer ion have the same m/z (m/z = 2,164.77 as calculated with their average mass in the case of PR^{D25N}), the greatest peak detected at m/z 2,164.51 was determined to represent two forms, a PR monomer and PR dimer, thus being $[PR^{D25N}]^{5+}$ and $[2PR^{D25N}]^{10+}$ (Fig. S2*A*). In the present report hereafter, we designate a monomer and a dimer ion of PR^{X} as $[PR^{X}]^{Y}$ and $[2PR^{X}]^{Y}$, respectively, where X denotes an amino acid substitution(s) and Y denotes a charge of ion. To determine whether the detected ions represented monomers and/or dimers, we examined multiply charged isotopologue clusters of PR^{D25N} using the Solarix FT-ICR MS (Bruker Daltonics) and analyzed the difference in m/z ratios of two adjacent isotope peaks ($\Delta m/z$) because monomer and dimer PR^{D25N} ions with the same m/z show different $\Delta m/z$ values in order of their charges (Figs. S2 and S3 and Table S1) (18). The results of isotopologue ion analysis, illustrated in Fig. S3 *A* and *B*, demonstrated that the ions observed at m/z 1,546.39 and 1,803.94 in Fig. S2*A* were +7 and +6 charged monomer PR^{D25N} ions ($[PR^{D25N}]^{7+}$ and $[PR^{D25N}]^{6+}$), respectively. The ions detected at m/z 2,164.51 in Fig. S2*A* represent a mixture of +5 charged PR^{D25N} monomers and +10 charged PR^{D25N} dimers, designated as $[PR^{D25N}]^{5+}$ and $[2PR^{D25N}]^{10+}$, respectively, as shown in Fig. S3*D*, where "2PR" denotes a cluster of PR dimers. The ions at m/z 1,967.84 and 2,404.91 in Fig. S2*A* represent +9 and +11 charged PR^{D25N} dimers ($[2PR^{D25N}]^{11+}$ and $[2PR^{D25N}]^{9+}$), respectively, as shown in Fig. S3 *C* and *E*.

We also constructed three mutated PR species containing amino acid substitutions at the active site (PR^{D29N}, PR^{T26A}, and PR^{R87K}), a C terminus-truncated mutant ($PR^{1\text{-}C95A}$), and a PR carrying L97A and F99A substitutions ($PR^{97/99}$) (6, 19). In Fig. 2*C*, two PR^{D29N} dimer ions ($[2PR^{D29N}]^{11+}$ and $[2PR^{D29N}]^{9+}$) were detected, whereas no dimer ions were detected with PR^{T26A} and PR^{R87K} (Fig. 2 *D* and *E*). Additional analyses of the isotopologue ion peaks with PR^{T26A} and PR^{R87K} confirmed the absence of dimer ions (Fig. S4 *A*–*F* and Table S1). Importantly, two $PR^{1\text{-}C95A}$ dimer ions ($[2PR^{1\text{-}C95A}]^{11+}$ and $[2PR^{1\text{-}C95A}]^{9+}$) were identified, although $PR^{1\text{-}C95A}$ monomer ion ($[PR^{1\text{-}C95A}]^{6+}$) was found to be a major peak (Fig. 2*F*). Two dimer ions were also detected in the case of $PR^{97/99}$, as shown in Fig. 3*C*. Considering that $[PR^{WT}]^{5+}$+$[2PR^{WT}]^{10+}$ representing monomers+dimers was found to be a major peak together with a minor peak of $[PR^{WT}]^{6+}$ in Fig. 2*A*, the $PR^{1\text{-}C95A}$ and $PR^{97/99}$ species were thought to have a significantly reduced but persistent ability to dimerize in comparison with PR^{WT}. Taken together, the data strongly suggest that the PR dimerization process consists of two distinct steps: (*i*) initial albeit weak intermolecular interactions occurring in the active site interface, constructing unstable or transient dimers, and (*ii*) subsequent interactions in the termini interface, resulting in the complete and tighter PR dimerization (Fig. 4).

In an attempt to examine the thermal stability of PR^{WT} and various mutated PR species mentioned above, we conducted

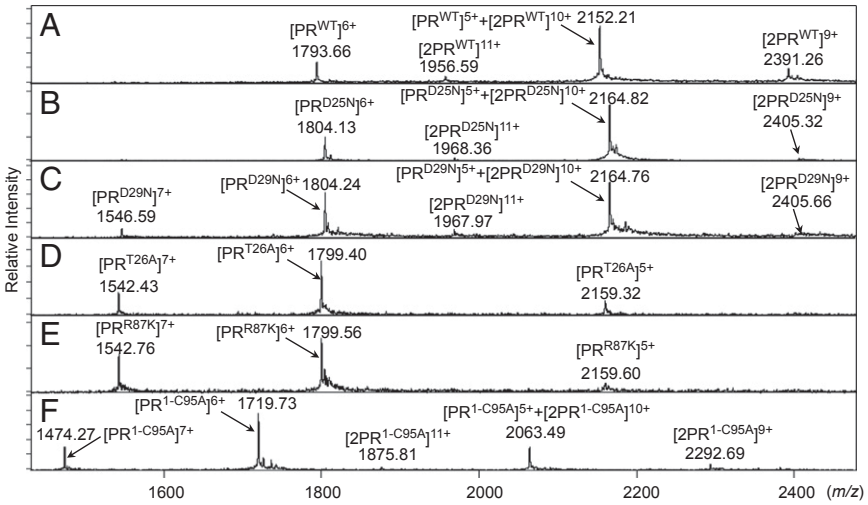

Fig. 2. ESI-MS spectra with PR^{D25N}, PR^{D29N}, PR^{T26A}, PR^{R87K}, and $PR^{1\text{-}C95A}$. (*A*) The ESI-MS spectrum of PR^{WT} (10 μM). (*B*–*F*) Results of ESI-MS analysis of each mutant (10 μM). (*B*) The ESI-MS spectrum of PR^{D25N} showed four peaks derived from its monomer and/or dimer ions. (*C*) PR^{D29N} showed five peaks including +11 or +9 charged dimer ions. (*D* and *E*) The ESI-MS spectra of PR^{T26A} and PR^{R87K}, respectively. The isotopologue ion peak analysis showed that all peaks detected in the ESI-MS spectra of PR^{T26A} and PR^{R87K} were derived from monomer ions (Fig. S4 and Table S1). (*F*) In the spectrum of $PR^{1\text{-}C95A}$, five peaks including the +11 and +9 charged dimer ions were seen. The average mass of PR^{WT}, PR^{D25N}, PR^{D29N}, PR^{T26A}, PR^{R87K}, and $PR^{1\text{-}C95A}$ are 10,755.76, 10,818.86, 10,818.86, 10,789.82, 10,791.83, and 10,312.24, respectively.

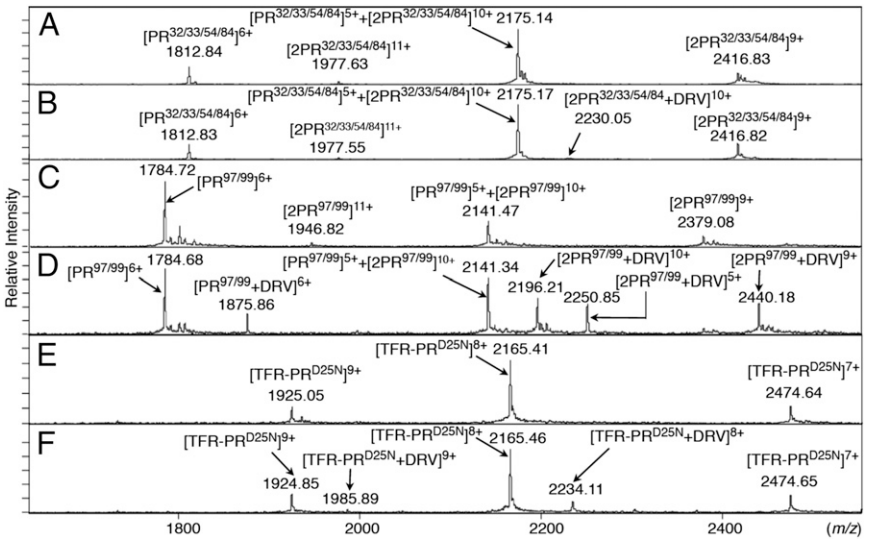

Fig. 3. ESI-MS spectra of $PR^{32/33/54/84}$, $PR^{97/99}$, and TFR-PR^{D25N}. (*A*) The ESI-MS spectrum of $PR^{32/33/54/84}$ (53.4 μM) without DRV. (*B*) The ESI-MS spectrum of $PR^{32/33/54/84}$ (55.6 μM) with DRV (400 μM). The addition of DRV showed only a small amount of DRV-bound $PR^{32/33/54/84}$ dimer ions, $[2PR^{32/33/54/84}+DRV]^{10+}$. (*C*) The ESI-MS spectrum of $PR^{97/99}$ (40.8 μM) in the absence of DRV. (*D*) The ESI-MS spectrum of $PR^{97/99}$ (40.3 μM) in the presence of DRV (120 μM). DRV binding to $PR^{97/99}$ yielded four additional peaks derived from $[PR^{97/99}+DRV]^{6+}$, $[2PR^{97/99}+DRV]^{10+}$, $[PR^{97/99}+DRV]^{5+}$, and $[2PR^{97/99}+DRV]^{9+}$. (*E*) The ESI-MS spectrum of TFR-PR^{D25N} (4.5 μM) without DRV. (*F*) The ESI-MS spectrum of TFR-PR^{D25N} (5.2 μM) with DRV (120 μM). Addition of DRV yielded two DRV-bound TFR-PR^{D25N} monomer ions, $[TFR\text{-}PR^{D25N}+DRV]^{9+}$ and $[TFR\text{-}PR^{D25N}+DRV]^{8+}$. The average masses of $PR^{32/33/54/84}$, $PR^{97/99}$, and TFR-PR^{D25N} are 10,870.92, 10,701.67, and 17,183.74, respectively.

differential scanning fluorimetry (DSF) (20). As illustrated in Fig. 5, the order of thermal stability was $PR^{WT} > PR^{D25N} > PR^{D29N} > PR^{32/33/54/84} > PR^{97/99} \sim PR^{T26A} > PR^{R87K} > PR^{1\text{-}C95A}$ (T_m; 53.37 > 52.18 > 51.02 > 50.17 > 48.22 ~ 48.12 > 47.02 > 44.46 °C, respectively). The difference in T_m values (ΔT_m) between PR^{D25N} and PR^{D29N} (1.16 °C) was less than ΔT_m between PR^{D25N} and $PR^{1\text{-}C95A}$ (7.72 °C), indicating that in terms of thermal stability, PR^{D25N} is closer to PR^{D29N} compared with the most unstable $PR^{1\text{-}C95A}$. Thus, PR^{D29N} monomer subunits are likely to interact at the active site interface and subsequently, at the termini interface, forming stable dimers. The DSF data, however, showed that T_m value of $PR^{97/99}$ (48.22 °C) was quite low compared with that of PR^{WT} (53.37 °C) and PR^{D29N} (51.02 °C), suggesting that $PR^{97/99}$ dimers are likely to be unstable. The T_m value of $PR^{1\text{-}C95A}$ was further lower (44.46 °C), suggesting that $PR^{1\text{-}C95A}$ dimers are also likely to be unstable (Fig. 5 *A* and *B*). Taking the ESI-MS and DSF results together, one can presume that the present ESI-MS assay detects both unstable (transient) and stable dimers. Furthermore, the present DSF data indicate that the stability of $PR^{97/99}$ and $PR^{1\text{-}C95A}$ dimers was lower than that of PR^{D25N} dimer (dimer dissociation constant; K_D = 1.3 μM), suggesting that the K_D values of transient dimers were higher than 1.3 μM (21). Thus, the present DSF data corroborate the above ESI-MS data showing that the HIV-1 PR dimerization process undergoes two steps (Fig. 4).

We previously reported that DRV inhibits not only proteolytic activity but also PR dimerization, whereas two FDA-approved anti-HIV-1 drugs, saquinavir (SQV) and nelfinavir (NFV), have no dimerization inhibition activity as examined with the FRET-based HIV-1 expression system (Fig. S1*A*) (13). To analyze the mechanism of the PR dimerization inhibition by DRV, we therefore examined the binding properties of DRV, SQV, and NFV with PR^{WT} (Fig. 6 *A*–*D*). The ESI-MS spectrum of PR^{WT} without drugs showed four peaks derived from differently charged ions, $[PR^{WT}]^{6+}$, $[2PR^{WT}]^{11+}$, $[PR^{WT}]^{5+}+[2PR^{WT}]^{10+}$, and $[2PR^{WT}]^{9+}$ (Fig. 6*A*). In the presence of DRV, four additional peaks appeared, ($[PR^{WT}+DRV]^{6+}$, $[2PR^{WT}+DRV]^{10+}$, $[PR^{WT}+DRV]^{5+}$, and $[2PR^{WT}+DRV]^{9+}$) (Fig. 6*B*). Additional analysis of the isotopologue ion peaks with PR^{D25N} in the presence of DRV confirmed the identity of monomer and dimer ions, as shown in Fig. S3 *F*–*I* and Table S2.

On the other hand, the binding of SQV to PR^{WT} yielded only two additional peaks, $[2PR^{WT}+SQV]^{10+}$ and $[2PR^{WT}+SQV]^{9+}$ (Fig. 6*C*), indicating that SQV binds only to PR^{WT} dimers, not to monomers. In the presence of NFV, as in the case of SQV, two additional peaks, $[2PR^{WT}+NFV]^{10+}$ and $[2PR^{WT}+NFV]^{9+}$, were identified (Fig. 6*D*). The relatively weak intensity of SQV- and NFV-bound PR^{WT} dimers is presumably due to their relatively low binding affinity to PR^{WT}, as previously demonstrated by Dierynk et al. (22). Taken together, these data indicate that SQV and NFV bind to PR^{WT} dimers but not to monomers, and DRV inhibits PR dimerization by binding to PR monomers in a one-to-one molar ratio.

Highly DRV-resistant HIV-1 isolates we previously generated in vitro (14) had acquired a unique combination of four amino acid substitutions (V32I/L33F/I54M/I84V), and DRV had decreased its binding to PR monomers containing such four amino acid substitutions (Fig. S1*B*) (14, 15). We therefore examined whether such four amino acid substitutions altered the binding profiles of DRV with PR, using ESI-MS. The ESI-MS spectrum of $PR^{32/33/54/84}$ refolded in the absence of DRV showed four

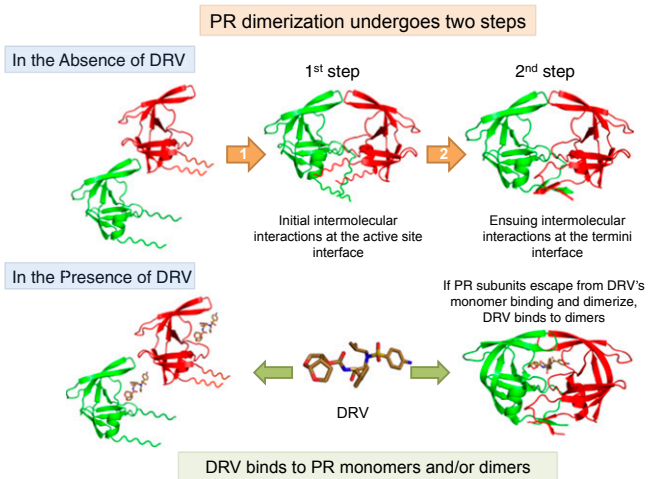

Fig. 4. The HIV-1 PR dimerization process undergoes two steps, and DRV inhibits the first step of PR dimerization by binding to PR monomers. PR subunits initially interact at the active site interface, generating unstably dimerized PR subunits, and subsequently the termini interface interactions occur, completing the dimerization process, generating stable PR dimers. DRV binds in the proximity of the active site interface of PR and blocks PR subunits dimerization. If PR subunits escape from the DRV's monomer binding and dimerize, DRV binds to PR dimers.

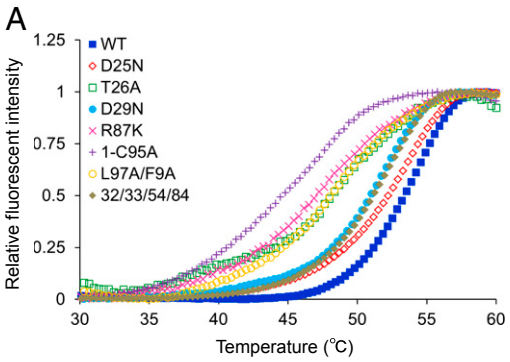

B

mutants	Tm (°C)
PR^{WT}	53.37±0.22
PR^{D25N}	52.18±0.24
PR^{T26A}	48.12±0.61
PR^{D29N}	51.02±0.22
$PR^{97/99}$	48.22±0.57
$PR^{1\text{-}C95A}$	44.46±0.69
$PR^{32/33/54/84}$	50.17±0.07

Fig. 5. Thermal stability of PR^{WT} and various mutated PR species determined using DSF. (*A*) Thermal denaturation, which was detected using SYPRO Orange, of PR^{WT}, PR^{D25N}, PR^{T26A}, PR^{D29N}, PR^{R87K}, $PR^{1\text{-}C95A}$, $PR^{L97A/F9A}$, and $PR^{32/33/54/84}$. (*B*) T_m values (the temperature at which the relative fluorescent intensity is 0.5) of each PR species.

peaks derived from five differently charged ions, $[PR^{32/33/54/84}]^{6+}$, $[2PR^{32/33/54/84}]^{11+}$, $[PR^{32/33/54/84}]^{5+}$+$[2PR^{32/33/54/84}]^{10+}$, and $[2PR^{32/33/54/84}]^{9+}$ (Fig. 3*A*). However, in the presence of DRV, only a substantially low peak representing DRV-bound $PR^{32/33/54/84}$ dimers, $[2PR^{32/33/54/84}+DRV]^{10+}$, was detected at *m/z* 2,230.05, and no DRV-bound PR monomers were detected (Fig. 3*B*). Thus, it seems that the loss of binding affinity to $PR^{32/33/54/84}$ in the monomeric form is greater than that in the dimeric form. Furthermore, we determined whether DRV binds to a mutated PR containing two substitutions (L97A/F99A; $PR^{97/99}$), which play important roles for the termini interface interactions but have no association with DRV resistance. The ESI-MS spectrum of $PR^{97/99}$ without DRV showed four peaks, $[PR^{97/99}]^{6+}$, $[2PR^{97/99}]^{11+}$, $[PR^{97/99}]^{5+}$+$[2PR^{97/99}]^{10+}$, and $[2PR^{97/99}]^{9+}$ (Fig. 3*C*). However, in the presence of DRV, four additional peaks appeared, $[PR^{97/99}+DRV]^{6+}$, $[2PR^{97/99}+DRV]^{10+}$, $[PR^{97/99}+DRV]^{5+}$, and $[2PR^{97/99}+DRV]^{9+}$ (Fig. 3*D*). Thus, L97 and F99 are not critical for DRV's monomer binding. The present data showed that the current ESI-MS method we used in this study is useful in detecting DRV's specific binding to PR^{WT}.

Finally, we asked whether DRV had an ability to bind to the PR precursor protein, Gag-Pol polyprotein, which is produced through the frame-shifting process in the Gag-encoding gene translation (Fig. S5 *A* and *B*) and subsequently maturates after the due excision through autoproteolysis (23–26). To examine the DRV binding to the PR precursor protein, a transframe precursor form of PR containing D25N substitution, TFR-PR^{D25N}, was constructed (Fig. S5*C*). In the absence of drugs, TFR-PR^{D25N} generated $[TFR\text{-}PR^{D25N}]^{10+}$, $[TFR\text{-}PR^{D25N}]^{9+}$, $[TFR\text{-}PR^{D25N}]^{8+}$, and $[TFR\text{-}PR^{D25N}]^{7+}$ (Fig. 3*E*), indicating that TFR-PR^{D25N} failed to dimerize, in line with the NMR data reported by Ishima et al. (19). In the presence of DRV two additional peaks, $[TFR\text{-}PR^{D25N}+DRV]^{8+}$ and $[TFR\text{-}PR^{D25N}+DRV]^{9+}$, appeared (Fig. 3*F*), indicating that DRV bound to TFR-PR^{D25N} monomers. In this regard, Agniswarmy et al. (27) have shown that the addition of C terminus four amino acids (PISP) to TFR-PR increases thermal stability of DRV-bound TFR-PR. In the present study we generated TFR-$PR^{D25N\text{-}7AA}$, which contained an additional seven N terminus amino acids of reverse transcriptase (7AA; PISPIET) at the C terminus of TFR-PR^{D25N}. The ESI-MS revealed that TFR-$PR^{D25N\text{-}7AA}$ formed dimers (Fig. S6*A*), suggesting that the addition of the seven amino acids allowed TFR-$PR^{D25N\text{-}7AA}$ to dimerize, probably by giving TFR-$PR^{D25N\text{-}7AA}$ proper conformation. The ESI-MS then showed that DRV binds to both TFR-$PR^{D25N\text{-}7AA}$ monomers and dimers (Fig. S6*B*). These results strongly suggest that the loss of dimerization ability of TFR-PR^{D25N} resulted in the loss of DRV's dimer binding.

Discussion

In the present study we constructed three "active site interface PR mutants" (PR^{T26A}, PR^{D29N}, and PR^{R87K}) and two "termini interface PR mutants" ($PR^{1\text{-}C95A}$ and $PR^{97/99}$) and determined their ESI-MS profiles. In the ESI-MS spectra, the peaks of PR^{D29N} monomers ($[PR^{D29N}]^{6+}$ and $[PR^{D29N}]^{7+}$) were greater than those of PR^{WT} ($[PR^{WT}]^{6+}$ and $[PR^{WT}]^{7+}$) (Fig. 2 *A* and *C*). The peaks of PR^{D29N} monomers ($[PR^{D29N}]^{6+}$ and $[PR^{D29N}]^{7+}$) were also greater than those of PR^{D29N} dimers ($[2PR^{D29N}]^{9+}$ and $[2PR^{D29N}]^{11+}$) (Fig. 2*C*). The same was true for the cases of $PR^{1\text{-}C95A}$ and $PR^{97/99}$ (Figs. 2*F* and 3*C*). These findings suggest that the dimers represent small components in the three mutated PR species. However, as assessed using the FRET-based HIV-1 expression assay, PR^{D29N} dimerization was apparently completely disrupted (13). Of particular note, the FRET-based system determines the FRET signal (CFP fluorescence after photobleaching/CFP fluorescence before photobleaching: $CFP^{A/B}$ ratio) in one cell at one time, accumulates ~20–30 cells' data, and obtains the average of the $CFP^{A/B}$ ratios. Then, if the average value is greater than 1.0, it is judged that FRET occurred, indicating that PR dimerization took place within the cell. However, there is variability in the $CFP^{A/B}$ ratios within the assay data, probably due to, but not limited to (*i*) unequal expression of PR proteins; (*ii*) uneven occurrence of protein–protein interactions (i.e., dimerization); and (*iii*) differing compartmentalization of the expressed PR species within the transfected cell population. Nevertheless, the FRET-based HIV-1 expression assay system only calls whether FRET occurred or did not occur. Thus, the FRET-based HIV-1 expression assay system inherently fails to identify the presence of a small amount of dimers or monomers. Therefore, in the case of PR^{D29N}, the FRET signal was determined as "not detected" (13). However, the ESI-MS system we used in the present study directly and more quantitatively identifies PR monomers and dimers. Thus, the ESI-MS system correctly recognized both a major fraction of PR^{D29N} monomers as well as a minor fraction of PR^{D29N} dimers. Accordingly, increasing the expression of PR^{D29N} by increasing the amount of plasmid for transfection does not increase the specific FRET-based signal, which we have confirmed in our initial conditioning phase of the construction of the system. Both PR^{T26A} and PR^{R87K} failed to dimerize as examined with the FRET-based HIV-1 expression assay, and no dimerized PR species were seen in the ESI-MS spectra (Fig. S4 and Table S1). When we examined the ESI-MS spectra of $PR^{1\text{-}C95A}$ and $PR^{97/99}$, the peaks of +6 charged monomer ions were much greater than in the PR^{WT} spectrum; however, PR dimer species were also present (Figs. 2*F* and 3*C*). Moreover, DSF analysis showed that $PR^{1\text{-}C95A}$ and $PR^{97/99}$ dimers were unstable (Fig. 5). Taking these data together, it is strongly suggested that the PR dimerization process undergoes two steps: (*i*) initial albeit weak intermolecular interactions occurring in the active site interface, and (*ii*) subsequent interactions

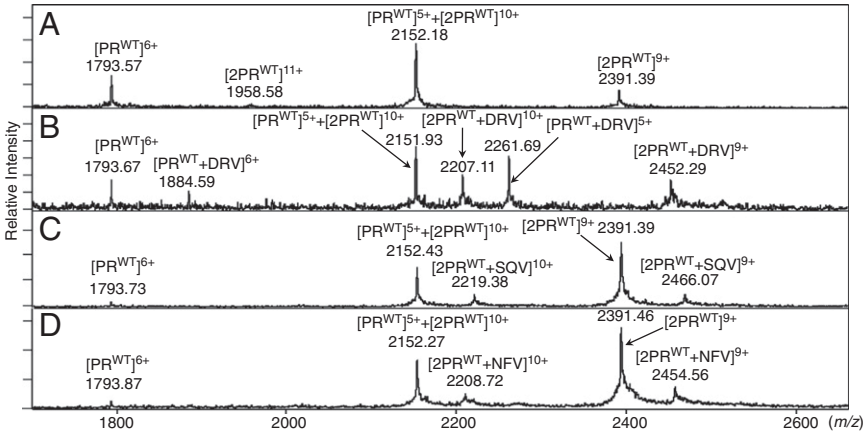

Fig. 6. The binding properties of DRV, SQV, and NFV to wild-type PR. (*A*) ESI-MS spectra of PR^{WT} (10.0 μM) in the absence of DRV, obtained by Bio-Tof-Q. (*B–D*) ESI-MS spectra of PR^{WT} in the presence of DRV, SQV, and NFV (all 120 μM); the final concentrations of PR^{WT} were 10.0, 9.5, and 14.4 μM, respectively. (*B*) Addition of DRV yielded four DRV-bound PR^{WT} ions, $[PR^{WT}+DRV]^{6+}$, $[2PR^{WT}+DRV]^{10+}$, $[PR^{WT}+DRV]^{5+}$, and $[2PR^{WT}+DRV]^{9+}$. (*C*) In the presence of SQV, two SQV-bound PR^{WT} dimer ions, $[2PR^{WT}+SQV]^{10+}$ and $[2PR^{WT}+SQV]^{9+}$, were observed, whereas SQV-bound PR^{WT} monomer ion were not seen. (*D*) Addition of NFV yielded two NFV-bound PR^{WT} dimer ions, $[2PR^{WT}+NFV]^{10+}$ and $[2PR^{WT}+NFV]^{9+}$, whereas no NFV-bound PR^{WT} monomer ions were present. The average mass of DRV, SQV, and NFV are 547.66, 670.85, and 567.31, respectively.

occurring in the termini interface, resulting in the complete and tight PR dimerization (Fig. 4).

In the present study, we also demonstrated that DRV binds to PR^{WT} monomers as well as dimers, whereas other "conventional" PIs, including SQV and NFV, bind only to dimers (Fig. 6 *A–D*), confirming that DRV uniquely has dual activity against PR^{WT}: inhibition of PR^{WT} dimerization and proteolytic activity as previously described (13). It is also noteworthy that the present data clearly showed that DRV binds to PR^{WT} monomer subunit in a one-to-one molar ratio.

We have previously selected highly DRV-resistant HIV-1 variants ($HIV_{DRV}{}^{R}$) and identified that $HIV_{DRV}{}^{R}$ had acquired a unique combination of four amino acid substitutions (V32I/L33F/I54M/I84V) in the proximity of the active site interface of its PR (Fig. 1) (14). In the present data DRV virtually completely failed to bind to $PR^{32/33/54/84}$ monomers, and only a small amount of DRV-bound $PR^{32/33/54/84}$ dimers was identified (Fig. 3*B*). However, L97A and F99A substitutions did not affect DRV's monomer and dimer binding (Fig. 3*D*). These results indicate that the binding domain in PR monomers for DRV is located distantly from the termini interface and is close to the active site interface, in line with the results of computational results reported by Huang et al. (28). Thus, the present ESI-MS analysis results strongly suggest that DRV blocks the first step of the PR dimerization process involving the active site interface, by binding to PR monomers in a one-to-one molar ratio (Fig. 4).

We have shown that once stable PR^{WT} dimers are formed, DRV no longer disrupts the dimers, as examined using the FRET-based assay (13). To ask whether DRV's binding to PR^{WT} monomers yields sufficient force to block PR^{WT} dimerization, the determination of the binding affinity of DRV for the folded monomers seems to be technically highly challenging. However, the present ESI-MS data showed that the amount of DRV-bound PR^{WT} monomers seemed to be greater than that of DRV-bound PR^{WT} dimers (Fig. 6*B*). Moreover, we determined the thermal stability of DRV-bound PR^{WT}, which apparently contains more DRV-bound PR^{WT} monomers than DRV-bound PR^{WT} dimers (Fig. 6*B*). As illustrated in Fig. S7, PR^{WT} was found to be highly stable as examined using the differential scanning fluorimetry (DSF), strongly suggesting that DRV fairly strongly binds to PR^{WT} monomer. The DSF data also suggested that DRV's binding to PR^{WT} monomers should have sufficient force to block PR^{WT} dimerization, inhibiting the formation of transient dimers. It is of note that if the formation of transient dimers (first step of the dimerization process) is blocked by DRV, the formation of stable dimers through the termini interface interactions (second step of the dimerization step) no longer occurs (Fig. 4). The determination of the exact binding site of PR monomer for DRV awaits further investigation, such as crystallographic analysis of PR monomer complexed with DRV and other dimerization inhibitors (13, 29, 30).

Louis et al. (24) have recently demonstrated that among nine FDA-approved PIs, DRV and SQV most potently block the autoproteolytic processing of the precursor construct (TFR-PR). Davis et al. (26) also demonstrated that among six FDA-approved HIV-1 PIs, DRV and SQV most potently block the initial step of autoproteolytic processing of Gag-Pol polyprotein by embedded dimerized PR. These data strongly suggest that DRV and SQV bind to TFR-PR, although the dynamics of the DRV binding remain elusive (26). In the present work DRV bound to TFR-$PR^{D25N-7AA}$ monomers and dimers (Fig. S6 *A* and *B*), in line with the data by Louis et al. (24), and our data strongly suggest that DRV blocks the autoproteolytic processing of Gag-Pol polyproteins through binding to the PR precursors (monomers and dimers) within the Gag-Pol polyprotein, contributing to DRV's potent antiretroviral activity against HIV-1. As for SQV, which has a greater K_D value (1.2×10^{-9} M) for binding to PR^{WT} than DRV (4.1×10^{-13} M) (22), Sayer and Louis (31) have shown that D25N substitution substantially decreases SQV's binding affinity to PR. Indeed, the present ESI-MS data also showed that SQV fails to bind to PR^{D25N}, TFR-PR^{D25N}, and TFR-$PR^{D25N-7AA}$ (Fig. S6*C* and S8 *A–C*). Thus the levels of SQV binding to these PR mutants carrying D25N substitution do not seem to be sufficient to be detected by ESI-MS.

A few groups have reported PR dimerization inhibitors targeting the terminal interface of PR (9–12). However, none of such inhibitors have been of clinical utility, probably because PR dimers, once formed, are highly stable to "de-dimerize" with the potent dimerization forces in the termini interface (13). On the other hand, the active site interface interactions play a critical role for PR dimerization, but the dimers formed are thought to be relatively unstable. Thus the development of new dimerization inhibitors targeting the active site interface would be highly suitable. It is also noteworthy that the ESI-MS approach is more quantitative than the FRET-based HIV-1 expression system, and we demonstrated two features: (*i*) DRV binds to PR^{WT} monomers and dimers, whereas (*ii*) DRV binds only to TFR-PR^{D25N} monomers. Thus, ESI-MS analysis is useful in analyzing how PR monomers and dimers act in the presence or absence of dimerization-targeting drugs. The new findings demonstrated in the present study should help understand the mechanism of HIV-1 PR inhibition and should also help develop novel and more potent PIs.

Materials and Methods

Vector Construction. The expression vectors containing the HIV-1 PR gene (pET-TFR-PR_{NL4-3}, pET-PR_{NL4-3}, and pET-$PR^{1\text{-}C95A}$) were constructed by using the In-Fusion HD Cloning Kit (Clontech). The other mutants (PR^{WT}, PR^{D25N},

PR^{T26A}, PR^{D29N}, PR^{R87K}, $PR^{32/33/54/84}$, and TFR-PR^{D25N}) were generated using the PrimeSTAR mutagenesis protocol (TaKaRa). More details are described in *SI Materials and Methods*.

FRET Procedure. The generation of the FRET-based HIV-1 expression system using CFP- and YFP-tagged HIV-1 PR-encoding plasmids we previously reported (13) is described in *SI Materials and Methods*.

Protein Preparation. The protein expression using plasmids we generated was induced by addition of 1 mM isopropyl β-D-thiogalactopyranoside. PR was purified by using buffer A (20 mM Tris, 1 mM EDTA, and 1 mM DTT), and buffer A containing 2 M Urea was used. The expressed PR was solubilized with 50 mM formic acids (pH 2.8). The unfolded PR refolded with a neutralizing buffer [100 mM ammonium acetate, pH 6.0, 2% (vol/vol) methanol]. More details are described in *SI Materials and Methods*.

Thermal Stability Analysis Using DSF. In the DSF analysis, the final concentration of refolded PR mutants was 7–10 μM. SYPRO Orange (Life Technologies) was then added to the PR solution (final concentration of SYPRO orange: 5×) (20). Thirty microliters of the PR solution was successively heated from 25 °C to 95 °C, and changes of the fluorescence intensity were documented by the real-time PCR system 7500 Fast (Applied Biosystems). More details are described in *SI Materials and Methods*.

Analysis with ESI-MS. MS spectra of PR^{D25N} with and without DRV were obtained using a Bio-Tof-Q ESI quadrupole time-of-flight mass spectrometer (Bruker Daltonics). For the isotopologue ion peak analysis, high-resolution mass spectrometry was performed on a Bruker SolariX 9.4T FT-ICR MS (for PR^{D25N}) or a Bruker SolariX 7T FT-ICR MS (for PR^{T26A} and PR^{R87K}). More details are described in *SI Materials and Methods*.

ACKNOWLEDGMENTS. This work was supported in part by a grant for the Global Education and Research Center Aiming at the Control of AIDS (Global Center of Excellence, supported by Monbu-Kagakusho); Promotion of AIDS Research from the Ministry of Health, Welfare, and Labor of Japan; a grant to the Cooperative Research Project on Clinical and Epidemiological Studies of Emerging and Reemerging Infectious Diseases (Renkei Jigyo, no. 78; Kumamoto University) of Monbu-Kagakusho (to H.M.); the Intramural Research Program of the Center for Cancer Research, National Cancer Institute, National Institutes of Health (H.M.); and by Extramural Grant GM53386 from the National Institutes of Health (to A.K.G.).

1. Wlodawer A, et al. (1989) Conserved folding in retroviral proteases: Crystal structure of a synthetic HIV-1 protease. *Science* 245(4918):616–621.
2. Babé LM, Rosé J, Craik CS (1995) Trans-dominant inhibitory human immunodeficiency virus type 1 protease monomers prevent protease activation and virion maturation. *Proc Natl Acad Sci USA* 92(22):10069–10073.
3. Weber IT (1990) Comparison of the crystal structures and intersubunit interactions of human immunodeficiency and Rous sarcoma virus proteases. *J Biol Chem* 265(18): 10492–10496.
4. Strisovsky K, Tessmer U, Langner J, Konvalinka J, Kräusslich HG (2000) Systematic mutational analysis of the active-site threonine of HIV-1 proteinase: Rethinking the "fireman's grip" hypothesis. *Protein Sci* 9(9):1631–1641.
5. Todd MJ, Semo N, Freire E (1998) The structural stability of the HIV-1 protease. *J Mol Biol* 283(2):475–488.
6. Ishima R, Torchia DA, Louis JM (2007) Mutational and structural studies aimed at characterizing the monomer of HIV-1 protease and its precursor. *J Biol Chem* 282(23): 17190–17199.
7. Louis JM, et al. (2003) Revisiting monomeric HIV-1 protease. Characterization and redesign for improved properties. *J Biol Chem* 278(8):6085–6092.
8. Louis JM, Ishima R, Torchia DA, Weber IT (2007) HIV-1 protease: Structure, dynamics, and inhibition. *Adv Pharmacol* 55:261–298.
9. Babé LM, Rosé J, Craik CS (1992) Synthetic "interface" peptides alter dimeric assembly of the HIV 1 and 2 proteases. *Protein Sci* 1(10):1244–1253.
10. Shultz MD, et al. (2004) Small-molecule dimerization inhibitors of wild-type and mutant HIV protease: A focused library approach. *J Am Chem Soc* 126(32):9886–9887.
11. Shultz MD, Chmielewski J (1999) Probing the role of interfacial residues in a dimerization inhibitor of HIV-1 protease. *Bioorg Med Chem Lett* 9(16):2431–2436.
12. Davis DA, et al. (2006) Inhibition of HIV-1 replication by a peptide dimerization inhibitor of HIV-1 protease. *Antiviral Res* 72(2):89–99.
13. Koh Y, et al. (2007) Potent inhibition of HIV-1 replication by novel non-peptidyl small molecule inhibitors of protease dimerization. *J Biol Chem* 282(39):28709–28720.
14. Koh Y, et al. (2010) In vitro selection of highly darunavir-resistant and replication-competent HIV-1 variants by using a mixture of clinical HIV-1 isolates resistant to multiple conventional protease inhibitors. *J Virol* 84(22):11961–11969.
15. Koh Y, et al. (2011) Loss of protease dimerization inhibition activity of darunavir is associated with the acquisition of resistance to darunavir by HIV-1. *J Virol* 85(19): 10079–10089.
16. Loo JA (2000) Electrospray ionization mass spectrometry: A technology for studying noncovalent macromolecular complexes. *Int J Mass Spectrom* 200(1-3):175–186.
17. Loo JA, et al. (1998) Application of electrospray ionization mass spectrometry for studying human immunodeficiency virus protein complexes. *Proteins* 33(Suppl 2): 28–37.
18. Senko MW, Beu SC, McLaffertycor FW (1995) Determination of monoisotopic masses and ion populations for large biomolecules from resolved isotopic distributions. *J Am Soc Mass Spectrom* 6(4):229–233.
19. Ishima R, Torchia DA, Lynch SM, Gronenborn AM, Louis JM (2003) Solution structure of the mature HIV-1 protease monomer: Insight into the tertiary fold and stability of a precursor. *J Biol Chem* 278(44):43311–43319.
20. Niesen FH, Berglund H, Vedadi M (2007) The use of differential scanning fluorimetry to detect ligand interactions that promote protein stability. *Nat Protoc* 2(9): 2212–2221.
21. Sayer JM, Liu F, Ishima R, Weber IT, Louis JM (2008) Effect of the active site D25N mutation on the structure, stability, and ligand binding of the mature HIV-1 protease. *J Biol Chem* 283(19):13459–13470.
22. Dierynck I, et al. (2007) Binding kinetics of darunavir to human immunodeficiency virus type 1 protease explain the potent antiviral activity and high genetic barrier. *J Virol* 81(24):13845–13851.
23. Sadiq SK, Noé F, De Fabritiis G (2012) Kinetic characterization of the critical step in HIV-1 protease maturation. *Proc Natl Acad Sci USA* 109(50):20449–20454.
24. Louis JM, Aniana A, Weber IT, Sayer JM (2011) Inhibition of autoprocessing of natural variants and multidrug resistant mutant precursors of HIV-1 protease by clinical inhibitors. *Proc Natl Acad Sci USA* 108(22):9072–9077.
25. Pettit SC, Everitt LE, Choudhury S, Dunn BM, Kaplan AH (2004) Initial cleavage of the human immunodeficiency virus type 1 GagPol precursor by its activated protease occurs by an intramolecular mechanism. *J Virol* 78(16):8477–8485.
26. Davis DA, et al. (2012) Activity of human immunodeficiency virus type 1 protease inhibitors against the initial autocleavage in Gag-Pol polyprotein processing. *Antimicrob Agents Chemother* 56(7):3620–3628.
27. Agniswamy J, Sayer JM, Weber IT, Louis JM (2012) Terminal interface conformations modulate dimer stability prior to amino terminal autoprocessing of HIV-1 protease. *Biochemistry* 51(5):1041–1050.
28. Huang D, Caflisch A (2012) How does darunavir prevent HIV-1 protease dimerization? *J Chem Theory Comput* 8(5):1786–1794.
29. Amano M, et al. (2013) GRL-0519, a novel oxatricyclic ligand-containing nonpeptidic HIV-1 protease inhibitor (PI), potently suppresses replication of a wide spectrum of multi-PI-resistant HIV-1 variants in vitro. *Antimicrob Agents Chemother* 57(5): 2036–2046.
30. Aoki M, et al. (2012) Loss of the protease dimerization inhibition activity of tipranavir (TPV) and its association with the acquisition of resistance to TPV by HIV-1. *J Virol* 86(24):13384–13396.
31. Sayer JM, Louis JM (2009) Interactions of different inhibitors with active-site aspartyl residues of HIV-1 protease and possible relevance to pepsin. *Proteins* 75(3):556–568.